RSC Advances

ROYAL SOCIETY OF CHEMISTRY

www.rsc.org/advances

Cite this: DOI: 10.1039/c0xx00000x

www.rsc.org/xxxxxx

ARTICLE TYPE

Larger π-Extended *anti*-/*syn*-Aroylenediimidazole Polyaromatic Compounds: Synthesis, Physical Properties, Self-Assembly, and Quasi-linear Conjugation Effect

Jianfeng Zhao,[a,c,e] Jen It Wong,[b] Junkuo Gao,[a] Gang Li,[a] Guichuan Xing,[d] Huacheng Zhang,[d] Tze Chien Sum,[d] Hui Ying Yang,[b] Yanli Zhao,[d] Staffan Lars Ake Kjelleberg,[e] Wei Huang,*[c] Say Chye Joachim Loo,*[a,e] Qichun Zhang*[a,e]

Received (in XXX, XXX) Xth XXXXXXXXX 200X, Accepted Xth XXXXXXXXX 200X
DOI: 10.1039/b000000x

Four π-extended *anti*-/*syn*-aroylenediimidazole (ADI) polyaromatic compounds (1, 2, 3, and 4) with 11- or 13- fused rings have been successfully synthesized *via* Tandem cyclocondensation reaction between tetraamines and naphthalene dicarboxylic monoanhydride monoimide. The observed optical bandgaps for 1-4 are 2.70 (458 nm), 2.34 (529 nm), 2.31 (537 nm), and 2.21 eV (561 nm), respectively, which is in accordance with the calculated bandgaps through DFT calculations for 1-4, which are 2.77, 2.49, 2.29, and 2.21 eV, respectively. Our results indicate that there are obvious *anti*-/*syn*- and π-extended effects in these molecules. The cyclic voltammetry (CV) measurements show that all compounds exhibit quasi-reversible reduction waves. The experimental LUMO levels from CV show an interesting zigzag-curved change (zigzag-shaped curve) in sequence, which matches well with those of theoretical calculation. Furthermore, the fitted decay lifetimes of 1-4 in $CHCl_3$ are 1.86, 1.32, 1.55, and 1.42 ns, which have the same trend as the above-mentioned zigzag-shaped curve. These trends are believed to be related to the intrinsically effective quasi-linear conjugation (QLC) with theoretically calculated quasi-linear length of 1.10 nm, 1.94 nm, 1.56 nm, and 2.40 nm, respectively. The successful synthesis and characterization of four soluble π-extended ADI polyaromatic compounds could provide us more diverse candidates for air-stable organic electronic devices.

For decades, larger π-extended acenes[1-4] have been strongly striding forward as the most prospective candidates for the applications in organic-semiconductor devices such as organic photovoltaic cells, [4] organic light-emitting diodes (OLEDs), [5] and organic field effect transistors (OFETs). [2b,6,7] Especially, conjugated acenes have been well-developed and some of them have been demonstrated to exhibit p-type characteristics with the hole mobility of thin films/crystals as high as 4.28/31.3 $cm^2V^{-1}s^{-1}$. [3c,8] By contrast, the performance of n-type heteroacenes are far lagged [2f,9] although some N-substituted acenes (oligoazaacenes) has already shown some decent mobilities in FETs. Very recently, a breakthrough in solution-processed air-stable n-type organic thin-film transistors with mobility of up to 3.50 $cm^2V^{-1}s^{-1}$ [10] has been reported. However, searching new organic conjugated systems to push up the electron mobility is still the main goal for most research groups.

Although the functionalization of parent frameworks with strong electron-withdrawn group such as –CN, –F, or –C=O, [1b,4b,11] have been explored to approach n-type materials, the tedious synthesis has posed a limitation for their further versatile applications. Alternatively, an effective strategy to realize n-type π-extended organic semiconductors is the replacement of CH groups in the backbones of oligoacenes with sp^2 N atoms. With appropriate arrangement (numbers or positions) of sp^2 N atoms in the backbones, [2f,12] the lowest unoccupied molecular orbitals (LUMO) could be optimized to fall between –4.0 and –4.5 eV for air stability[9f,9h,13] without oxidative degradation. [9d,14]

As one of the most facile and efficient synthetic routines to approach larger electron deficient aromatic π-systems, versatile Tandem cyclocondensation with *ortho*-positioned carboxyls and amines has been widely employed, including diketone/hydroxyl-diamine,[2f,9,15] aldehyde-diamine, methylene/ketone-amine,[17] carboxylic group-amine, [18] anhydride-amines[11d,19] and so on.[20] Here, we are interested in exploring the anhydride-amines method to construct as large as 11- or 13-ring fused π-extended aroylenediimidazole (ADI) polyaromatic compounds through cyclocondensation reactions between aromatic tetraamines and commercially available or easily-prepared n-type monomers aromatic monoanhydrides. In this paper, four novel ADI polyaromatic compounds (Scheme 1): **1-4** have been synthesized and physical properties have been fully characterized.

Results and Discussion

Synthesis

Four novel ADI polyaromatic compounds **1-4** were successfully synthesized *via* the Tandem cyclocondensation reaction among benzene-1,2,4,5-tetraamine, phenazine-2,3,7,8-tetraamine hydrochloride salts,[21] and the naphtanlenetetracarboxylic monoimide monoanhydride (NIA) [22] according to the similar reported procedure with slight modification (Scheme 1). [23] All as-prepared compounds **1-4** have been chromatographically purified and fully characterized by ^1H NMR, MALDI-TOF mass and high-resolution mass spectrometry. Note that it is not possible to obtain their ^{13}C NMR spectr due to their poor solubility. In addition, their physical properties such as ultraviolet–visible spectra (UV-Vis), photoluminescence spectra (PL), cyclic voltammetry (CV), fluorescence lifetime measurement, theoretic calculation, field

emission scanning electron microscopy (FE-SEM), and electroluminescence device (EL) of **2** nanofibers are also presented in this report.

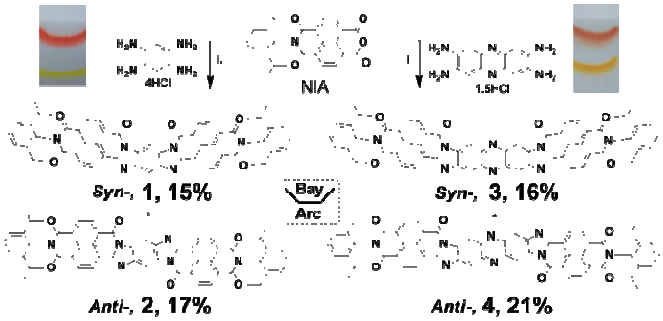

Scheme 1. The Synthetic route of four ADI polyaromatic compounds: 1-4. Reaction condition: i. Pyridine, reflux, 6h. Inset: the pictures of newly separated samples on TLC-SiO_2 plates ($CHCl_3$/MeOH).

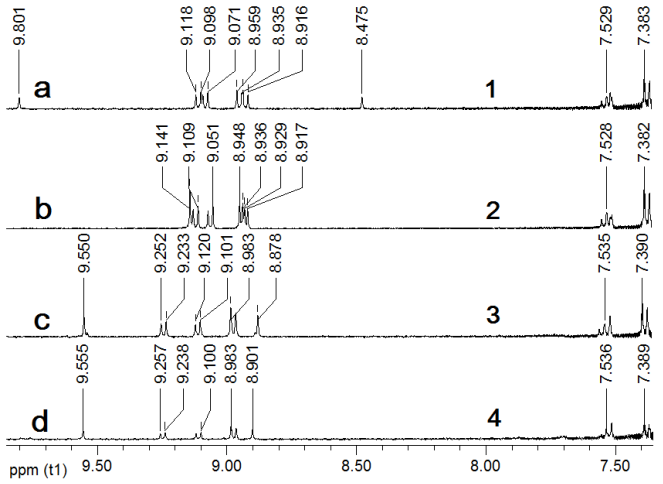

Figure 1. ^{1}H NMR spectra of separated ADI polyaromatic compounds **1** (a), **2** (b), **3** (c), and **4** (d) in $CDCl_3$ solutions.

The ^{1}HNMR spectra (in $CDCl_3$, 400 MHz) of four ADI polyaromatic compounds **1-4** are shown in Figure 1. The two aromatic proton signals with single peak at 9.80 (s, 1H) and 8.48 ppm (s, 1H) (Figure 1a) belong to outer arc and inner bay protons of diimidazolo-fused phenylene in *syn*-type **1**, respectively. The aromatic proton signal with single peak at 9.14 ppm (s, 2H) (Figure 1b) belongs to the two central protons of diimidazolophenylene in *anti*-type **2** with central symmetry. The aromatic proton signals with triple and double peaks from 7.51 to 7.38 ppm belong to end-capped phenylenes for both **1** and **2**. Other signals with double or multi peaks ranging from 9.12 to 8.92 ppm distribute to their naphthalene groups. For **3** and **4**, the two signals with single peak at 9.55 ppm (s, 1H) and 8.87 ppm (s, 1H) in Figure 1c and 9.56 ppm (s, 1H) and 8.90 ppm (s, 1H) in Figure 1d belong to the protons of central phenazine moieties of **3**/**4**. Since the difference (0.67 ppm) between 9.55 ppm (s, 1H) and 8.87(8) ppm (s, 1H) in Figure 1c is larger than that (0.65 ppm) between 9.56 ppm (s, 1H) and 8.90 ppm (s, 1H) in Figure 1d, we believe that Figure 1c belongs to **3** while Figure 1d is assigned to **4**. Such assignment can be explained by following reasons: (1) **4** has a more homogeneous π-electron delocalized system than **3**, and (2) the protons close to sp^3-N atoms should appear at the highfield while the protons close to sp^2-N atoms should appear at the lowfield. For **3,** the two arc protons both adjacent to two sp^2-*N* atoms and two bay protons adjacent to two sp^3-N atoms lead to the broader fieldshift distance between them comparing to **4** system. The other signals come from naphthanlenes and phenylenes matched well with **1** and **2**. The distribution of four molecular structures was also easily confirmed by the symmetry-determined polarity as shown the inset in Scheme 1. Thus, it is not surprising to investigate that *anti*-type **2** and **4** exhibit smaller polarity and run faster on TLC plates than that of *syn*-type **1** and **3**, respectively.

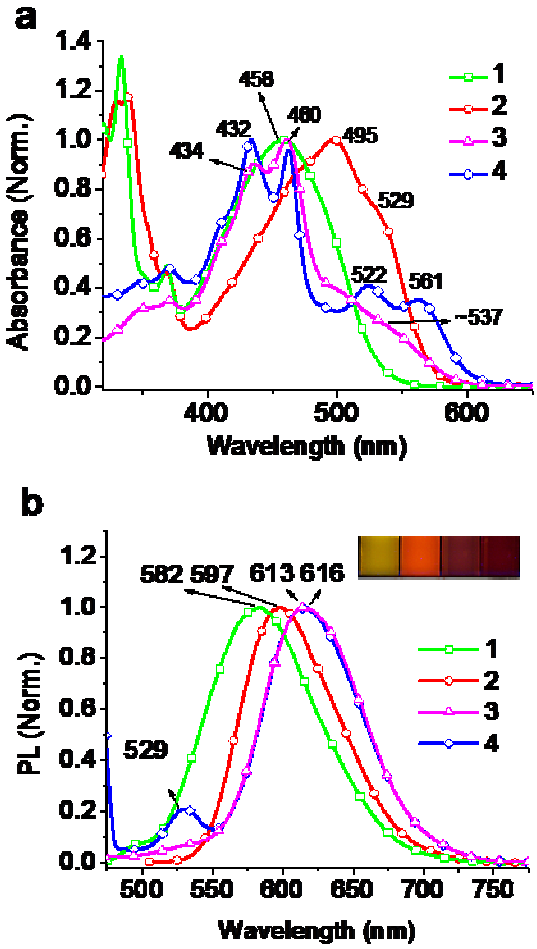

Figure 2. (a) Normalized absorption spectra of four compounds **1-4** in THF solutions (1×10^{-5} mol/L); (b) Normalized photoluminescence spectra (excited at 458, 495, 459, and 460 nm, respectively) of four compounds in THF solutions (1×10^{-5} mol/L). Green line-**1**, red line-**2**, pink line-**3**, blue line-**4**.

Optical properties

As shown the inset in Scheme 1, after separation by thin layer chromatography with $CHCl_3$-MeOH as mobile phase and SiO_2 as stationary phase, the molecular layer of **1-4** absorbed on SiO_2 exhibit different colors (yellow, bright red, orange, and red-brown, respectively). This phenomenon is ascribed to the structural *anti*-/*syn*-effect. *Anti*-isomers **2** and **4** have well-dislocating π-electrons and lower energy levels exhibiting their deeper colors than their corresponding isomers. Meanwhile, longer π-extended **3** and **4** show deeper colors due to the enhanced intramolecular charge transfer (ICT) of larger π-aggregation compared to those of **1** and **2**. It indicates that a

zigzag-shaped color changing trend exist from yellow, red, orange to red-brown of **1-4**, respectively.

Figure 2a and 2b present the normalized UV-Vis absorption and photoluminescence (PL) spectra of **1-4** in THF solutions (1×10^{-5} mol/L). For absorption, the shoulder peak at 529 nm of *anti*-type **2** can be ascribed to the ICT with an obviously redshifted maximum absorption peak at 495 nm compared to that at 458 nm of *syn*-type **1** without ICT absorption due to the shorter linear π-conjugation. Similarly, *anti*-type **4** also exhibits more obvious ICT absorption peaks at 522 and 561 nm probably resulted from the electron transfer between sp^3-*N* atoms and electron-deficient imidazolo-fused phenazine and carboxyl naphthalenes compared to the germinating peaks at ~501 and ~537 nm of *syn*-type **3**. The calculated optical bandgaps for **1-4** are 2.70 eV (458 nm), 2.34 eV (529 nm), 2.31 eV (~537 nm), and 2.21 eV (561 nm) with a gradually decreasing trend, respectively.

As shown in Figure 2b, normalized photoluminescence spectra (excited at 458, 495, 459, and 460 nm, respectively) of **1-4** in THF solutions (1×10^{-5} mol/L) show the gradually redshifted emission peaks from 582, 597, 608, and 611 nm with different fluorescence colors (yellow, orange, red, and red). The maximum emission peaks at 582 and 597 nm of **1** and **2** showed apparently blueshifted wavelength than that at 613 and 616 nm of **3** and **4**. These results indicate that π-extended backbones and *anti*-type configuration could adjust the absorption, photoluminescence and optical bandgap effectively, as typical π-extension effect and *anti*-/*syn*- effect.

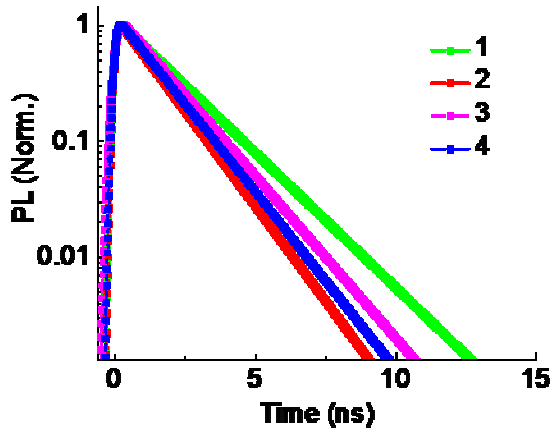

Figure 3. Single-exponential fittings (lines) for **1-4** in $CHCl_3$ (4.0×10-5 mol/L); green-**1**, red-**2**, pink-**3**, blue-**4** (Excited at 400 nm). Values of χ2 are 0.9685, 0.9692, 0.9467, and 0.9822, respectively.

Fluorescence decay measurement

The normalized emission decay curves for **1-4** in THF (1×10^{-5} mol/L) and their corresponding decay fittings are shown in Figure 3. The intensity decays with time *via* a single-exponential function, with well-defined value of χ^2 are 0.9685, 0.9692, 0.9467, and 0.9822, and fitted decay lifetimes for **1-4** at 1.86, 1.32, 1.55, and 1.42 ns, respectively. These fitted lifetimes show a trend that the exciton photoluminescence lifetimes gradually change as the zigzag-shaped curves as shown in Figure 3. Among them, the *syn*-type **1**/**3** exhibit longer lifetimes comparing to those of *anti*-type **2**/**4**, which is ascribed to the configuration-determined longer effective quasi-linear conjugation (QLC) of the former pair than the latter, namely, the typical *anti*-/*syn*- effect. Moreover, π-extended **3**/**4** showing shorter lifetime than that of **1**/**2** is clearly caused by the longer QLC of the former than the latter π-extension effect. [22b] This zigzag-curved change might be explained by the length of effective QLC. Especially, although the molecular size of **3** is larger than that of **2**, but the effective QLC of **2** is longer than **3** (1.55 ns) leading to the shorter lifetime of **2** (1.32 ns).

Table 1. Physical properties of four ADI polyaromatic compoundss **1-4**.

Entries	$E_{1/2}^{red}$(V)[a]	LUMO (eV)[b]	HOMO (eV)[c]	E_{gap}/λ_{max} (eV)[d]/nm	LUMO(eV)[e]	HOMO(eV)[e]	E_{gap} (eV)[e]
1	−0.84	−3.56	−6.26	2.70	−3.48	−6.24	2.77
2	−0.74	−3.66	−6.00	2.34	−3.59	−6.08	2.49
3	−0.78	−3.62	−5.93	2.31	−3.58	−5.85	2.29
4	−0.66	−3.74	−5.95	2.21	−3.63	−5.84	2.21

[a] Obtained from cyclic voltammograms. Reference electrode: Ag/AgCl. [b] Calculated from cyclic voltammograms. [c] Calculated according to the formula $E_{LUMO} = -[4.4 + E_{1/2}^{red}]$ eV, $E_{HOMO} = E_{LUMO}-E_{gap}$. [d] Optical band gap, $E_{gap} = 1240/\lambda_{max}$ of the peaks at 458 nm, 529 nm, 537 nm, and 561 nm, respectively; [e] Obtained from theoretical calculations.

Cyclic Voltammetry

The electrochemical properties of ADI azaacenes **1-4** were performed in $CHCl_3$ in a standard three-electrode electrochemical cell using tetrabutyl-ammonium hexafluorophosphate (Bu_4NPF_6, TBAPF) (0.1 mol/L) as electrolyte, Ag/AgCl as reference electrode, Pt as working electrode and counter electrode (Pt wire). As shown in Figure 4 and Table 1, all ADI azaacenes **1-4** exhibit one quasi-reversible reduction wave. It is also indicated that four ADI azaacenes **1-4** are intrinsic n-type organic semiconductors due to the absent oxidation peaks. The half-wave reduction potentials for **1-4** are −0.84, −0.74, −0.78, and −0.66 V, respectively. Furthermore, according to the empirical equation $E_{LUMO} = -[4.4 + E_{1/2}^{red}]$ eV, [15,24] the lowest unoccupied molecular orbital (LUMO) energy levels were calculated to be −3.56, −3.66, −3.62, and −3.74 eV. *Anti*-type structures of **2** and **4** have a big effect on the value of HOMO and LUMO levels comparing to *syn*-type structures of **1** and **3**. It is worthy to note that the LUMOs decrease with increasing backbone length as *syn*-type **1** *vs* **3** and *anti*-type **2** *vs* **4**, namely, as π-extension effect and *snti/syn* effect. Moreover, *anti*-type **2** shows a lower LUMO level than *syn*-type **4**. These results indicated that this zigzag-curved change might be ascribed to the intrinsically effective QLC length.

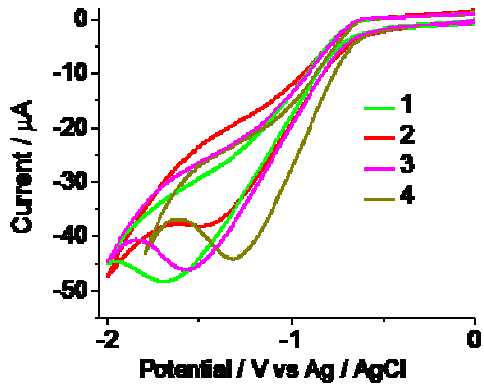

Figure 4. Cyclic Voltammetry curves of **1-4** in $CHCl_3$ solution containing 0.1 mol/L TBAPF electrolyte. Scanning rate: 100 mV/s. green line-**1**, red line-**2**, pink line-**3**, brown line-**4**.

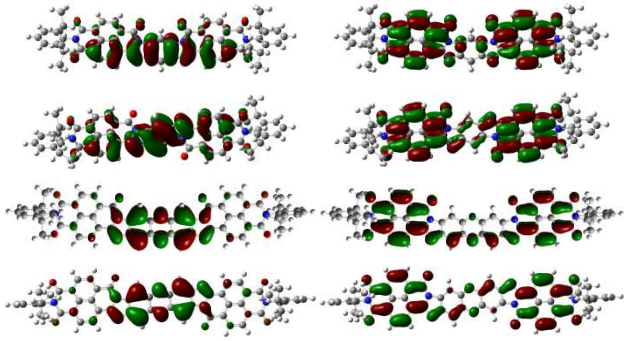

Figure 5. Models of molecular orbital for the HOMO (left column) and LUMO (right column) of ADI azaacenes **1** (a), **2** (b), **3** (c), and **4** (d).

Calculated from the optical bandgap and LUMO levels (See Table 1), the HOMO levels of **2**, **3**, and **4** ranging from −5.93 to −6.00 eV were higher than the value of azapetancenes (−6.03~−6.14 eV), [15] but lower than the value of pentacene (−5.14 eV) [25] and hexacene (−4.96 eV). [3c] By contrast, four ADI azaacenes **1-4** have lower LUMO levels (−3.56~−3.74 eV) than those of pentacene (−3.37 eV) and hexacene (−3.56 eV). [3a,18] Especially, the LUMO level of **4** (−3.74 eV) gets close to the air-stable limitation range (–4.0-–4.5 eV). [9d,9f,9h,13a-c,14] All these data could support that **1-4** might possess reasonable stability for the electron injection and transportation in device.[26] We believe that π-extension effect and *Anti/Syn* effect could play an important role in the molecular design and physical properties' tuning. To this point, *anti-type* configuration takes an obvious advantage over the *anti*-type one.

Theoretical calculation

All the electronic structures of **1-4** were theoretically calculated and optimized using density functional theory (DFT) at the B3LYP/6-31G* level.[27] At the same level, the ground state frontier molecular orbitals of the optimized molecules were also calculated (See Figure 5). The HOMO and LUMO orbitals of **1** and **2** and LUMO of **3** and **4** are all delocalized on the whole ADI backbones. But the HOMO of **3** and **4** mainly delocalized on the diimidazolophenazine framework without naphthalene groups. Especially, **3** exhibits more homogeneous delocalization with low energy due to *anti*-type structure as a quasi-linear channel for ICT.

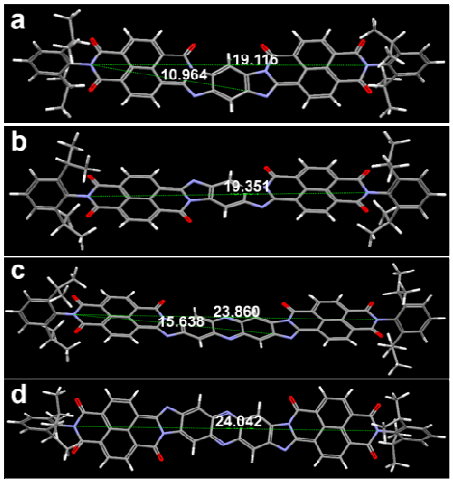

Figure 6. The theoretical calculated lengths: 1.10 nm, 1.94 nm, 1.56 nm, and 2.40 nm of quasi-linear conjugated backbone moieties of **1** (a), **2** (b), **3** (c), and **4** (d), respectively.

The calculated HOMO and LUMO levels and the bandgaps of **1-4** are matched very well with the experimental results, which are summarized in Table 1. Especially, the change of theoretical LUMO levels with the value of −3.48, −3.59, −3.58, and −3.63 eV from **1** to **4** also appears as a zigzag-shaped curve. This special change matches very well with the change of theoretically calculated length of effective conjugated backbone moieties so-called as quasi-linear backbone length as 1.10, 1.94, 1.56, and 2.40 nm of **1-4**, respectively, not with the gradually increased molecular conjugated backbone length (1.91, 1.93, 2.39, and 2.40 nm, Figure 6) or whole molecular length (2.97, 3.00, 3.45, and 3.47 nm, Figure S10).

As shown in Figure 7, the experimental results and theoretical calculation of **1-4** not only suggest the existence of typical π-extension effect and *anti-*/*syn*- effect, but also support the effective QLC induced zigzag-curved change of various intrinsically physical properties (e.g. different colors, fluorescence decay lifetimes, theoretically calculated and experimentally measured LUMO values).

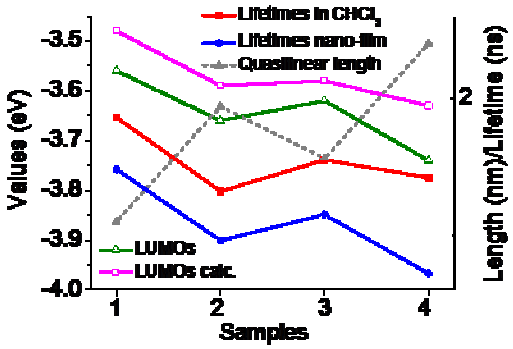

Figure 7. The zigzag-shaped curve of the relationship between structures and physical properties of ADI azaacences **1-4**.

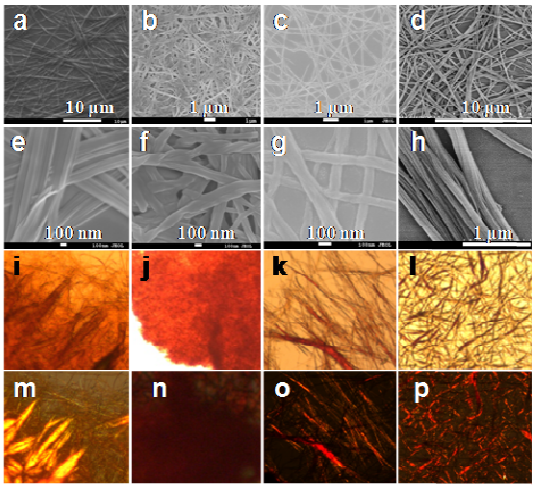

Figure 8. FE-SEM, magnified FE-SEM, POM and normal optical images of abundant self-assembled nanostructures of 1-4: nanobelts of **1** (a, e, i, and m); nanofibers of **2** (b, f, j, and n); nanowires of **3** (c, g, k, and o); nanobundles of **4** (d, h, i, and p); the optical and POM images of nanostructures (magnification: 16×20).

Self-assembly and electroluminescence device

The planar π-extended conjugation of **1-4** could allow them self-assembling into kinds of nanostructure by the slow evaporation of the corresponding solutions (e.g. THF for **1**,

MeOH-$CHCl_3$ (5:1, V/V) for **2** and **4**, hexane-*o*-dichlorbenzene (5:1, V/V) for **3**). Figure 8a, 8c, 8e, and 8g present field emission scanning electron microscopy (FE-SEM) images of as-prepared **1-4** nanobelts, nanofibers, nanowires, and nanobundles. The as-prepared nanostructures have widths or diameters in the range of ~50–400 nm and lengths ranging from tens to hundreds of micrometers. Figure 9e, 9f, 9g and 9h show the magnified images of the typical nanostructures (~50 nm). The optical and polarized optical microscopy (POM) images indicated that these four nanostructures are quasi-crystalline and stack anisotropically (Figure 8i-8p).

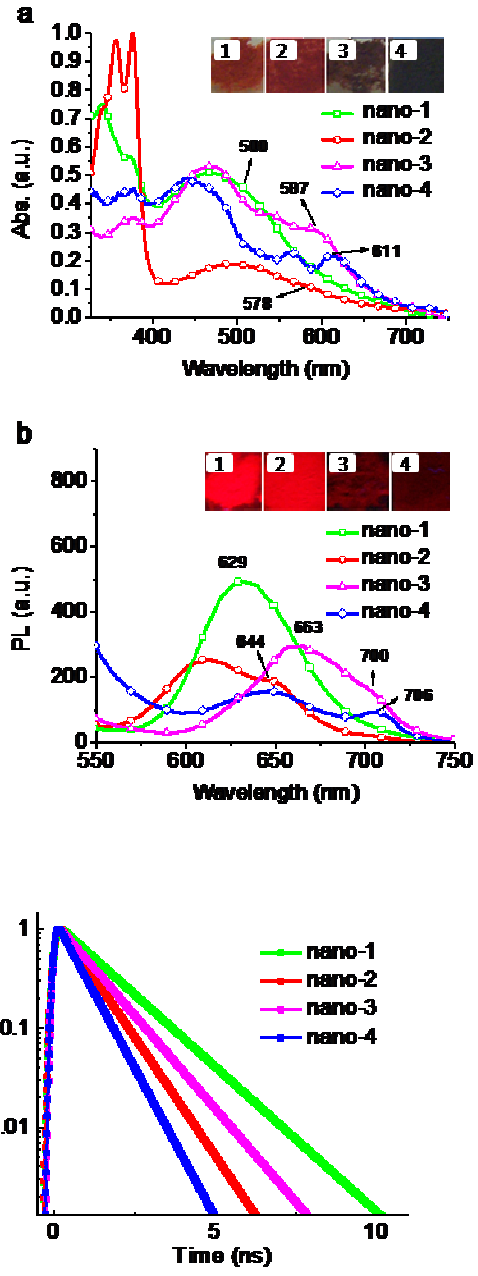

Figure 9. The absorption (a) and photoluminescence (a.u.) spectra of the dispersed solution in MeOH (b); insert pictures: color of the aggregates of **1-4** nanostructures and photoluminescence of their dropcast films (UV lamp, 365 nm); green line-1, red line-2, pink line-3, blue line-4; (c) Single-exponential fittings (lines) for the films of **1-4** nanostructures; green-**1**, red-**2**, pink-**3**, blue-**4** (Excited at 400 nm). Values of $\chi 2$ are 0.9972 (nano-1), 0.9954 (nano-**2**), 0.9781 (nano-3), and 0.9820 (nano-**4**).

As shown in Figure 9, the absorption spectra of the nanostructures of **1-4** exhibit obviously self-assembly induced ~40-50 nm redshift of the maximum absorbed peaks from 458, 529, 537, and 561 nm (in solution) to 500, 578, 587, and 611 nm (in nanostructure forms), respectively (Figure 2). Meanwhile, photoluminescence spectra of the films of nanostructures on glasses show the gradually redshifted emission peaks from 582, 597, 608, and 611 nm (in solution) to 629, 644, 700, and 706 nm (in nanostructure forms) with fluorescence color of orange, orange-red, red, and deep red, respectively, which indicates that intermolecular π-π stacking and the planar π-extended conjugation synergically predominate the final color of aggregates. Beside of these, the red-shifted absorption and photoluminescence of nanostructures of **1-4** suggest the formation of *J*-type aggregation through π-π stacking. [28,29] As shown in Figure 9c, the single-exponential fittings for the fluorescence decay lifetimes of the drop cast films of **1-4** nanostructures were also given as 1.48, 0.96, 1.15, and 0.72 ns, respectively, with obviously QLC induced zigzag-curved change. The values of χ^2 are 0.9972 (nano-**1**), 0.9954 (nano-**2**), 0.9781 (nano-**3**), and 0.9820 (nano-**4**).

Furthermore, a protocol heterojunction sandwich-like organic light-emitting device (OLED) using **2** nanofibers exampled as an active layer was fabricated. Figure 10a illustrates the schematic diagram of as-fabricated LED device containing layers of ITO/**2** nanofibers/p-SiC/Al (10 nm)/Ti (80 nm)/Al (380 nm)/ITO. The Al/Ti/Al layers were firstly formed by *e*-beam evaporation on the *p*-SiC and then furnace annealed at 1000 °C for 5 min protected by argon for an alloying heat treatment. After that, the water-dispersed nanofibers were drop-cast on the substrate and air-dried. Afterward, the substrate was annealed at 70°C under N_2 atmosphere for 2h. In the final step, ITO glass was directly pressed against the layer of nanofibers to form the top contact.

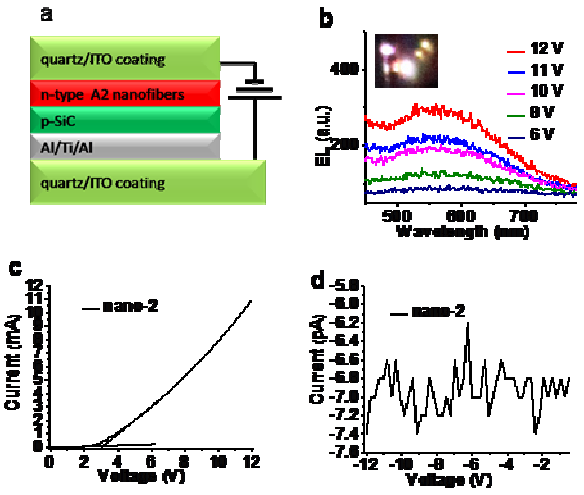

Figure 10. (a) Schematic diagram of the sandwich-like OLED structure: quartz/ITO/nano-**2**/p-SiC/Al (10 nm)/Ti (80 nm)/Al (380 nm)/ITO/quartz; (b) EL spectrum of the electron deficient 2 nanofibers/p-SiC heterojunction LED biased at various forward voltages (6-12V) with inserted turn-on image of OLED taken at 11 V; (c) and (d) Current–voltage characteristics of the same OLED device under the forward and the reverse bias, respectively.

Figure 10b presents the electroluminescence (EL) spectra of the **2** nanofibers/p-SiC heterojunction light emitting device biased at different forward voltages. An image of the EL device at forward bias of 11 V was taken and inserted in Figure 10b. When a constant forward bias of 11 V was biased, the detected current increased from 9.97 mA to 10.10 mA. A constant voltage was applied on the layer of nanofibers for all EL measurement, and the EL responding spectrum were measured by a photomultiplier detector equipped with a monochromator and collected from the optical fiber. The EL spectra showed broad emission spectra with a broad peak at ~561 nm with peak width of ~47 nm at intensity of 318 a.u. probably resulted from the aroylenediimidazole π-conjugated backbone with hole-electron recombination. Only the substrate zone with Al/Ti/Al contact area in the device gives the dotted light emitting phenomena. Meanwhile, there was no light emission observed for this heterojunction OLED when a reverse bias was applied. [30]

The current–voltage (*I-V*) characteristic of the device under forward and reverse bias was shown in Figure 10c and 10d, respectively. From Figure 10c, the heterojunction LEDs had a turn-on voltage of ~3.1 V and it is supported that the *I-V* curve exhibits a rectifying diode property and the use of n-type organic nanofibers as the electron injection layer could give an effective and low cost candidate to replace those inorganic thin-film layered devices.

Conclusions

In conclusion, four novel ADI polyaromatic compounds **1-4** have been successfully synthesized from easily available compounds or intermediates *via* an aromatic anhydride-diamine Tandem cyclocondensation. It is worthy to note that 13-ring **3** and **4** are one of the longest linear-shape n-type aroylenediimidazole/imide derivatives. [4b,7a,7b,11a,19i,31] They have been fully studied by photophysical measurements, electrochemical methods, theoretical calculation, and fluorescence lifetimes with zigzag-curved change due to the effective QLC. In addition, the typical *anti*-type effect, π-extension effect and predominately π-π stacked driven force synergically lead to the formation of abundant nanostructures, one of which has been successfully employed as the active layer in the OLED device. Our results could offer an effective way to design and approach promising larger π-extended n-type materials for air-stable organic electronic devices.

Experimental Section

Materials

7-(2,6-Diisopropylphenyl)-1*H*-isochromeno[6,5,4-*def*]isoquino-line-1,3,6,8(7*H*)-tetraone (NIA) [22] was prepared according to the reported literatures[19i,23] from the reaction between isochromeno[6,5,4-*def*]isochromene-1,3,6,8-tetraone (**a**) and 2,6-diisopropylaniline (**b**). Phenazine-2,3,7,8-tetraamine hydrochloride salt was prepared from benzene-1,2,4,5-tetraamine hydrochloride salt (**c**). [15,21] Compounds **a**, **b** and **c** were purchased from Sigma-Aldrich companies. All solvents were used without further purification.

General synthesis

NIA (~0.6 mmol) (Figure S9) and corresponding tetraamine hydrochloride salt (0.25 mmol) was mixed into pyridine (10 ml) and refluxed for 6h. After the reaction finished, pyridine was removed by rotary evaporation and the residue was purified firstly using silica-gel column chromatography and then preparative thin layer chromatography with chloroform/methanol (35:1 for **1/2**, 25:1 for **3/4**) to afford **1** (35 mg, 15%) and **2** (39 mg, 17%) as red solid powder, **3** (41 mg, 16%) and **4** (54 mg, 21%) as reddish brown and dark brownish-green powder, respectively.

1: ^{1}H NMR ($CDCl_3$, 400 MHz): δ 9.80 (s, 1H), 9.12 (d, *J*=7.78 Hz, 2H), 9.07 (d, *J*=7.70 Hz, 2H),8.96 (d, *J*=7.63 Hz, 2H), 8.94 (d, *J*=7.79 Hz, 2H), 8.48 (s, 1H), 7.53 (t, J=7.49 Hz, 2H), 7.38 (d, *J*=8.39 Hz, 4H), 2.75 (t, *J*=6.85 Hz, 4H), 1.19 (s, 12H), 1.18 (s, 12H). HRMS (ESI) *m*/*z*: M + H^+ C58H44N6O6 calcd. 920.3322; found 921.3387;

2: ^{1}H NMR ($CDCl_3$, 400 MHz): δ 9.14 (s, 2H), 9.13 (d, *J*=7.67 Hz, 2H), 9.07 (d, *J*=7.60 Hz, 2H), 8.95-8.93 (d, *J*=7.54 Hz, 2H), 8.94-8.92 (d, *J*=7.62 Hz, 2H), 7.53 (t, *J*=7.80 Hz, 2H), 7.38 (d, *J*=8.07 Hz, 4H), 2.75 (t, *J*=7.68 Hz, 4H), 1.20 (d, *J*=1.31 Hz, 12H), 1.18 (d, *J*=1.26 Hz, 12H). HRMS (ESI) *m*/*z*: M + H^+ C58H44N6O6 calcd. 920.3322; found 921.2242;

3: ^{1}H NMR ($CDCl_3$, 400 MHz): δ 9.55 (s, 2H), 9.25 (d, *J*=7.68 Hz, 2H), 9.10 (d, *J*=7.53 Hz, 2H), 8.98 (d, *J*=7.68 Hz, 4H), 8.87 (s, 2H), 7.54 (t, *J*=8.10 Hz, 2H), 7.39 (d, *J*=7.66 Hz, 4H), 2.75 (t, *J*=6.96 Hz, 4H), 1.24 (d, *J*=3.95 Hz, 12H), 1.20 (d, *J*=6.77 Hz, 12H). HRMS (ESI) *m*/*z*: M + H^+ C64H46N8O6 calcd. 1022.3540; found 1023.3851;

4: ^{1}H NMR ($CDCl_3$, 400 MHz): δ 9.56 (s, 2H), 9.26 (d, *J*=7.38 Hz, 2H), 9.10 (d, *J*=7.66 Hz, 2H), 8.98 (d, *J*=7.53 Hz, 4H), 8.90 (s, 2H), 7.54 (t, *J*=7.37 Hz, 2H), 7.39 (d, *J*=7.40 Hz, 4H), 2.75 (t, *J*=7.06 Hz, 4H), 1.25 (d, *J*=3.82 Hz, 12H), 1.20 (d, *J*=6.85 Hz, 12H). HRMS (ESI) *m*/*z*: M + $2H^+$ C64H46N8O6 calcd. 1022.3540; found 1024.3485.

Methods

Solution ^{1}H NMR spectra were measured on a Bruker ARX 400 spectrometer. The UV-Vis absorption and fluorescence spectra of **1-4** were recorded on Shimadzu UV-2501 and RF-5301 spectrophotometer, respectively. MS were collected on MALDI TOF2 AXIMA mass spectrometer. And HiRes- MALDI TOF MS spectra were recorded on a Waters Q-Tof premier TM mass spectrometer. Fluorescence decay lifetimes were measured by exciting the samples in $CHCl_3$ (10^{-5} mol/L) using a laser flash photolysis spectrometer (LKS.60, Applied Photophysics), equipped with a Q-switched Nd:YAG laser (Brilliant B, Quantel), a 150 W pulsed Xe lamp, and a R928 photomultiplier, was used to record nanosecond-difference absorption spectra. Samples were excited at 400 nm, and each time-resolved trace was acquired by averaging 10 laser shots at a repetition rate of 1 Hz. The room temperature fluorescence decay was conducted by exciting the samples in $CHCl_3$ (10^{-5} mol/L) with 400-nm, 150-fs laser pulses. These laser pulses were generated from a Coherent TOPAS-C optical parametric amplifier that was pumped using a 1 kHz Coherent Legend^{TM} regenerative amplifier, which is seeded by a 80 MHz Coherent Vitesse^{TM} oscillator. The laser pulses were focused by a lens (f = 25 cm) on the solution sample in a 2-mm-thick quartz cell. The emission from the samples was collected at a backscattering angle of 150° by a pair of lenses and directed into an Optronis Optoscope^{TM} streak camera system which has an ultimate temporal resolution of 10 ps.

The nanostructures of **1-4** (ADIs) were prepared as follows: 1 mg of ADIs was solved in 20 ml THF, MeOH-$CHCl_3$ (5:1, V/V), hexane-dichlorbenzene (5:1, V/V), MeOH-$CHCl_3$ (5:1, V/V), respectively. The mixture was stirred for 2h and filtrated due to the weak solubility of ADIs. The transparent solutions were kept in Al-foil sealed bottles/tubes and standstill at room temperature for several weeks. Nanostructures were formed at the bottom of the bottles/tubes. The as-prepared samples were coated with platinum in an ion coater for 30 s before the SEM investigation. The sizes and shapes of the nanostructures were observed on a FE-SEM (JSM-7600F, JEOL) at an accelerating voltage of 5 kV. Optical image was recorded by the Polarizing Microscope Olympus BX53. Electrochemistry was carried out with a CHI 600C potentiostat, employing a platinum button (diameter: 1.6 mm; area 0.02 cm^2), a platinum wire and a 0.01 M Ag/AgCl (Ag/Ag^+) as working, counter and reference electrode, respectively. 0.1 M of

tetrabutylammonium hexafluorophosphate ($TBAPF_6$) in $CHCl_3$ was used as the electrolyte.

Device Fabrication

The electroluminescence devices were fabricated. The typical fabrication method of the heterojunction LED was shown as follows: The HF-cleaned p-SiC substrate was coated with a metal contact (size of about 2 × 2 mm^2), which consisted of a layer of 10 nm Al film, then ~80 nm thick Ti film and a layer of ~380 nm thick Al film, by using *e* beam evaporation at room temperature. Water-dispersed **2** nanofibers were drop-cast on the opposite side surface of metal-electrode-deposited p-SiC substrate. The top of the **2** nanofibers was covered by the ITO coated quartz substrate, which was used as n-type **2** nanofibers contact. The EL spectra of the heterojunction LED were measured by connecting the anode and cathode of a rectangle pulse voltage source (with repetition rate and pulse width of 7.5 Hz and 80 ms, respectively) to the ITO coated quartz substrate and Al (10 nm)/Ti (80 nm)/Al (380 nm)/ metal contact on the p-SiC, respectively. Light was collected from the uncoated side of the quartz substrate by an objective lens.

Acknowledgements

Q.Zhang acknowledges financial support from AcRF Tier 1 (RG 16/12) and Tier 2 (ARC 20/12 and ARC 2/13) from MOE, the CREATE program (Nanomaterials for Energy and Water Management) from NRF, and the New Initiative Fund from NTU, Singapore; J.Loo acknowledges NMRC-EDG grant (EDG09may011) and SCELSE project (M020070110); W.Huang acknowledges the National Basic Research Program of China (2009CB930601), National Natural Science Foundation of China (21003706, 21274064, 21144004, 60876010, 61177029, 20774043, 20704023, and 20974046). G. C. Xing and T. C. Sum acknowledge the financial support by the Singapore National Research Foundation through the Competitive Research Programme under Project No. NRF-CRP5-2009-04 and the Singapore-Berkeley Research Initiative for Sustainable Energy (SinBerRISE) CREATE Programme.

Notes and references

[a] *School of Materials Science and Engineering, Nanyang Technological University, 50 Nanyang Avenue, Singapore 639798, Singapore, Fax: (+) 65-67909081, E-mail: qczhang@ntu.edu.sg, JoachimLoo@ntu.edu.sg*
[b] *Pillar of Engineering Product Development, Singapore University of Technology and Design, 20 Dover Drive, Singapore 138682, Singapore*
[c] *Institute of Advanced Materials, Nanjing University of Technology, 5 Xinmofan Road, Nanjing, 211816, China, E-mail: iamwhuang@njut.edu.cn*
[d] *School of Physical and Mathematical Sciences, Nanyang Technological University, 1 Nanyang Walk, Singapore, 637616, Singapore*
[e] *Singapore Centre on Environmental Life Sciences Engineering (SCELSE), Nanyang Technological University, Singapore*

1 (a) J. Mei, Y. Diao, A. L. Appleton, L. Fang, Z. Bao, *J. Am. Chem. Soc.* 2013, **135**, 6724; (b) C. L. Wang, H. L. Dong, W. P. Hu, Y. Q. Liu, D. B. Zhu, *Chem. Rev.* 2012, **112**, 2208; (c) J. W. Liu, H. W. Liang, S. H. Yu, *Chem. Rev.* 2012, **112**, 4770; (d) S. S. Zade, M. Bendikov, *Angew. Chem. Int. Ed.* 2010, **49**, 4012; (e) A. L. Appleton, S. M. Brombosz, S. Barlow, J. S. Sears, J. L. Bredas, S. R. Marder, U. H. F. Bunz, *Nat. Commun.* 2010, **1,** 91; (f) J. E. Anthony, *Angew. Chem. Int. Ed.* 2008, **47**, 452; (g) J. E. Anthony, *Chem. Rev.* 2006, **106**, 5028; (h) M. Bendikov, F. Wudl, D. F. Perepichka, *Chem. Rev.* 2004, **104**, 4891; (i) J. B. Li, Q. Zhang, *Synlett* 2013, 24, 686; (j) G. Li, Y. C. Wu, J. K. Gao, J. B. Li, Y. Zhao, Q. Zhang, *Chem. Asian J.* 2013, **8**, 1574; (k) G. Li, K. Zheng, C. Y. Wang, K. S. Leck, F. Z. Hu, X. W. Sun, Q. Zhang, *ACS Appl. Mater. Interfaces* 2013, **5**, 6458; l) Y. Zhang, D. Hanifi, E. Lim, S. Chourou, S. Alvarez, A. Pun, A. Hexemer, B. Ma, Y. Liu, *Adv. Mater.* 2013, DOI: 10.1002/adma.201304032; (m) J. Xiao, C. D. Malliakas, Y. Liu, F. Zhou, G. Li, H. Su, M. G. Kanatzidis, F. Wudl, Q. Zhang *Chem. Asian J.* 2012, **4**, 672.

2 (a) X. Feng, F. Iwanaga, J.-Y. Hu, H. Tomiyasu, M. Nakano, C. Redshaw, M. R. J. Elsegood, T. Yamato, *Org. Lett.* 2013, **15**, 3594; (b) H. Li, G. Giri, J. B.-H. Tok, Z. Bao, *MRS Bulletin* 2013, **38**, 34; (c) E. D. Głowacki, M. Irimia-Vladu, M. Kaltenbrunner, J. Gsiorowski, M. S. White, U. Monkowius, G. Romanazzi, G. P. Suranna, P. Mastrorilli, T. Sekitani, S. Bauer, T. Someya, L. Torsi, N. S. Sariciftci, *Adv. Mater.* 2013, **25**, 1563; (d) D. E. Jiang, S. Dai, *J. Phys. Chem. A* 2008, **112**, 332; (e) M. Winkler, K. N. Houk, *J. Am. Chem. Soc.* 2007, **129**, 1805; (f) M. Bendikov, H. M. Duong, K. Starkey, K. N. Houk, E. A. Carter, F. Wudl, *J. Am. Chem. Soc.* 2004, **126**, 7416; (g) K. N. Houk, P. S. Lee, M. Nendel, *J. Org. Chem.* 2001, **66**, 5517; (h) C. A. Di, J. Li, G. Yu, Y. Xiao, Y. L. Guo, Y. Q. Liu, X. H. Qian, D. B. Zhu, *Org. Lett.* 2008, **10**, 3025; (i) P. M. Beaujuge, J. M. J. Fréchet, *J. Am. Chem. Soc.* 2011, **133**, 20009; (j) J. Xiao, Y. Divayana, Q. Zhang, H. M. Doung, H. Zhang, F. Boey, X. W. Sun, F. Wudl *J. Mater. Chem*. 2010, **20**, 8167; (k) Q. Zhang, Y. Divayana, J. Xiao, Z. Wang, E. R. T. Tiekink, H. M. Doung, H. Zhang, F. Boey, X. W. Sun, F. Wudl, *Chem. Eur. J.* 2010, **16**, 7422; (l) H. M. Duong, M. Bendikov, D. Steiger, Q. Zhang, G. Sonmez, J. Yamada, F. Wudl, *Org. Lett.* 2003, **5**, 4433.

3 (a) S. Chen, F. S. Raad, M. Ahmida, B. R. Kaafarani, S. H. Eichhorn, *Org. Lett.* 2013, **15**, 558; (b) J. C. Xiao, H. M. Duong, Y. Liu, W. X. Shi, L. Ji, G. Li, S. Z. Li, X. W. Liu, J. Ma, F. Wudl, Q. Zhang, *Angew. Chem. Int. Ed.* 2012, **51**, 6094; (c) M. Watanabe, Y. J. Chang, S. W. Liu, T. H. Chao, K. Goto, M. M. Islam, C. H. Yuan, Y. T. Tao, T. Shinmyozu, T. J. Chow, *Nature Chem.* 2012, **4**, 574; (d) N. A. Minder, S. Ono, Z. Chen, A. Facchetti, A. F. Morpurgo, *Adv. Mater.* 2012, **24**, 503; (e) B. Purushothaman, M. Bruzek, S. R. Parkin, A. F. Miller, J. E. Anthony, *Angew. Chem. Int. Ed.* 2011, **50**, 7013; (f) I. Kaur, M. Jazdzyk, N. N. Stein, P. Prusevich, G. P. Miller, *J. Am. Chem. Soc.* 2010, **132**, 1261; (g) I. Kaur, N. N. Stein, R. P. Kopreski, G. P. Miller, *J. Am. Chem. Soc.* 2009, **131**, 3424; (h) D. Chun, Y. Cheng, F. Wudl, *Angew. Chem. Int. Ed.* 2008, **47**, 8380; (i) M. M. Payne, S. R. Parkin, J. E. Anthony, *J. Am. Chem. Soc.* 2005, **127**, 8028; (j) A. S. Molinari, H. Alves, Z. Chen, A. Facchetti, A. F. Morpurgo, *J. Am. Chem. Soc.* 2009, **131**, 2462; (k) U. H. F. Bunz, J. U. Engelhart, B. D. Lindner, M. Schaffroth, *Angew. Chem. Int. Ed.* 2013**, 52**, 3810.

4 (a) A. A. Gorodetsky, M. Cox, N. J. Tremblay, I. Kymissis, C. Nuckolls, *Chem. Mater.* 2009**, 21**, 4090; (b) H. Li, F. S. Kim, G. Ren, E. C. Hollenbeck, S. Subramaniyan, S. A. Jenekhe, *Angew. Chem. Int. Ed.* 2013, **52** (21), 5513-5517.

5 (a) J. C. Xiao, S. W. Liu, Y. Liu, L. Ji, X. W. Liu, H. Zhang, X. W. Sun, Q. Zhang, *Chem. Asian J.* 2012**, 7**, 561; (b) H. B. Liu, Y. L. Li, S. Q. Xiao, H. Y. Gan, T. G. Jiu, H. M. Li, L. Jiang, D. B. Zhu, D. P. Yu, B. Xiang, Y. F. Chen, *J. Am. Chem. Soc.* 2003, **125**, 10794; (c) H. B. Liu, J. L. Xu, Y. J. Li, Y. L. Li, *Acc. Chem. Res.* 2010, **43**, 1496; (d) J. Peet, A. J. Heeger, G. C. Bazan, *Acc. Chem. Res.* 2009, **42**, 1700; (e) Y. B. Guo, Q. X. Tang, H. B. Liu, Y. J. Zhang, Y. L. Li, W. P. Hu, S. Wang, D. B. Zhu, *J. Am. Chem. Soc.* 2008, **130**, 9198; (f) H. Klauk, U. Zschieschang, J. Pflaum, M. Halik, *Nature* 2007, **445** , 745; (g) H. Y. Gan, H. B. Liu, Y. J. Li, Q. Zhao, Y. L. Li, S. Wang, T. G. Jiu, N. Wang, X. R. He, D. P. Yu, D. B. Zhu, *J. Am. Chem. Soc.* 2005, **127**, 12452.

6 (a) Z. Yan, B. Sun, Y. Li, *Chem. Commun.* 2013, **49**, 3790; (b) T. Lei, J.-H. Dou, X.-Y. Cao, J.-Y. Wang, J. Pei, *J. Am. Chem. Soc.* 2013, **135**, 12168; (c) H. Jiang, K. K. Zhang, J. Ye, F. Wei, P. Hu, J. Guo, C. Liang, X. Chen, Y. Zhao, L. E. McNeil, W. Hu, C. Kloc, *Small* 2013, **9**, 990; (d) Y. Lin, Y. Li, X. Zhan, *Chem. Soc. Rev.* 2012, **41**, 4245; (e) T. Lei, J.-H. Dou, J. Pei, *Adv. Mater.* 2012, **24**, 6457; (f) I. G. Lezama, A. F. Morpurgo, *MRS Bulletin* 2013, **38**, 51; (g) W. Hu, Z. Bao, K. Müllen, *J. Mater. Chem.* 2012, **22**, 4134.

7 (a) T. V. Pho, F. M. Toma, M. L. Chabinyc, F. Wudl, *Angew. Chem. Int. Ed.* 2013**, 52**, 1446; (b) H. Herrera, P. de Echegaray, M. Urdanpilleta, M. J. Mancheno, E. Mena-Osteritz, P. Bauerle, J. L. Segura, *Chem. Commun.* 2013, **49**, 713; (c) Z. Sun, Q. Ye, C. Y. Chi, J. S. Wu, *Chem. Soc. Rev.* 2012, **41**, 7857; (d) J. Shao, J. Chang, C. Chi, *Org. Biol. Chem.* 2012, **10**, 7045; (e) L. M. Klivansky, D. Hanifi, G. Koshkakaryan, D. R. Holycross, E. K. Gorski, Q. Wu, M. Chai, Y. Liu, *Chem. Sci.* 2012, **3**, 2009; (f) M. Wang, Y. Li, H. Tong, Y. X. Cheng, L. X. Wang, X. B. Jing, F. S. Wang, *Org. Lett.* 2011, **13** , 4378; (g) R. Juarez, M. M. Oliva, M. Ramos, J. L. Segura, C. Aleman, F. Rodriguez-Ropero, D. Curco, F. Montilla, V.

Coropceanu, J. L. Bredas, Y. B. Qi, A. Kahn, M. C. R. Delgado, J. Casado, J. T. L. Navarrete, *Chem. Eur. J.* 2011, **17**, 10312.
8 H. Minemawari, T. Yamada, H. Matsui, J. Tsutsumi, S. Haas, R. Chiba, R. Kumai, T. Hasegawa, *Nature* 2011**, 475** , 364-367.
9 (a) Q. Miao, *Synlett* 2012, 326; (b) B. D. Lindner, J. U. Engelhart, M. Märken, O. Tverskoy, A. L. Appleton, F. Rominger, K. I. Hardcastle, M. Enders, U. H. F. Bunz, *Chem. Eur. J.* 2012, **18**, 4627; (c) O. Tverskoy, F. Rominger, A. Peters, H.-J. Himmel, U. H. F. Bunz, *Angew. Chem. Int. Ed.* 2011, **50**, 3557; (d) B. D. Lindner, J. U. Engelhart, O. Tverskoy, A. L. Appleton, F. Rominger, A. Peters, H. J. Himmel, U. H. F. Bunz, *Angew. Chem. Int. Ed.* 2011, **50**, 8588; (e) U. H. F. Bunz, *Pure Appl. Chem.* 2010, **82**, 953; (f) J. E. Anthony, A. Facchetti, M. Heeney, S. R. Marder, X. W. Zhan, *Adv. Mater.* 2010, **22**, 3876; (g) U. H. F. Bunz, *Chem. Eur. J.* 2009, **15**, 6780; (h) A. Lv, S. R. Puniredd, J. Zhang, Z. Li, H. Zhu, W. Jiang, H. Dong, Y. He, L. Jiang, Y. Li, W. Pisula, Q. Meng, W. Hu, Z. Wang, *Adv. Mater.* 2012, **24**, 2626; (i) Q. Zhang, J. Xiao, Z. Y. Yin, H. M. Duong, F. Qiao, F. Boey, X. Hu, H. Zhang, F. Wudl , *Chem. Asian. J.* 2011, **6**, 856.
10 F. Zhang, Y. Hu, T. Schuettfort, C.-A. Di, X. Gao, C. R. McNeill, L. Thomsen, S. C. B. Mannsfeld, W. Yuan, H. Sirringhaus, D. Zhu, *J. Am. Chem. Soc.* 2013, **135**, 2338.
11 (a) Z. Sun, K.-W. Huang, J. Wu, *Org. Lett.* 2010, **12**, 4690; (b) Z. Sun, K.-W. Huang, J. Wu, *J. Am. Chem. Soc.* 2011, **133**, 11896; (c) Y. Li, W.-K. Heng, B. S. Lee, N. Aratani, J. L. Zafra, N. Bao, R. Lee, Y. M. Sung, Z. Sun, K.-W. Huang, R. D. Webster, J. T. López Navarrete, D. Kim, A. Osuka, J. Casado, J. Ding, J. Wu, *J. Am. Chem. Soc.* 2012, **134**, 14913; (d) M. Zhu, J. Zhang, G. Yu, H. Chen, J. Huang, Y. Liu, *Chem. Asian J. 2*012, **7**, 2208.
12 Z. Liang, Q. Tang, R. Mao, D. Liu, J. Xu, Q. Miao, *Adv. Mater.* 2011, **23**, 5514.
13 L. Jiang, H. L. Dong, W. P. Hu, *J. Mater. Chem.* 2010, **20**, 4994.
14 (a) B. D. Lindner, J. U. Engelhart, M. Marken, O. Tverskoy, A. L. Appleton, F. Rominger, K. I. Hardcastle, M. Enders, U. H. F. Bunz, *Chem. Eur. J.* 2012, **18**, 4627; (b) A. L. Appleton, S. M. Brombosz, S. Barlow, J. S. Sears, J.-L. Bredas, S. R. Marder, U. H. F. Bunz, *Nat. Commun.* 2010, **1**, 91.
15 (a) G. Li, J. Gao, F. Hu, Q. Zhang, *Tetrahedron Lett.*, 2014,**55**,282. (b) P.-Y. Gu, F. Zhou, J. Gao, G. Li, C. Wang, Q.-F. Xu, Q. Zhang, J.-M. Lu, *J. Am. Chem. Soc.* 2013, **135**, 14086; (c) G. Li, Y. Wu, J. Gao, J. Li, Y. Zhao, Q. Zhang, *Chem. Asian J.* 2013, **8**, 1574; (d) G. Li, G. Long, W. Chen, F. Hu, Y. Chen, Q. Zhang, *Asian J. Org. Chem.* 2013, **2,** 852; (e) G. Li, K. Zheng, C. Wang, K. S. Leck, F. Hu, X. W. Sun, Q. Zhang, *ACS Appl. Mater. & interface* 2013, **5**, 6458; (f) C. Wang, G. Li, Q. Zhang,*Tetrahedron Lett.* 2013, **54**, 2633; (g) G. Li, Y. C. Wu, J. K. Gao, C. Y. Wang, J. B. Li, H. C. Zhang, Y. Zhao, Y. L. Zhao, Q. Zhang, *J. Am. Chem. Soc.* 2012, **134**, 20298; (h) G. Li, H. M. Duong, Z. Zhang, J. Xiao, L. Liu, Y. Zhao, H. Zhang, F. Huo, S. Li, J. Ma, F. Wudl Q. Zhang, *Chem. Comm.* 2012, **48**, 5974; (i) G. Li, A. A. Putu, J. Gao, Y. Divayana, W. Chen, Y. Zhao, X. W. Sun, Q. Zhang, Asian *J. Org. Chem.* 2012, **1**, 346.
16 J. Y. Chen, J. P. Qu, Y. Q. Zhang, Y. X. Chen, N. Liu, B. H. Chen, *Tetrahedron* 2013, **69**, 316.
17 (a) C. J. Tonzola, M. M. Alam, W. Kaminsky, S. A. Jenekhe, *J. Am. Chem. Soc.* 2003, **125**, 13548; (b) E. Ahmed, T. Earmme, G. Q. Ren, S. A. Jenekhe, *Chem. Mater.* 2010, **22**, 5786.
18 (a) S. Geib, S. C. Martens, U. Zschieschang, F. Lombeck, H. Wadepohl, H. Klauk, L. H. Gade, *J. Org. Chem.* 2012, **77**, 6107; (b) S. C. Martens, U. Zschieschang, H. Wadepohl, H. Klauk, L. H. Gade, *Chem. Eur. J.* 2012, **18**, 3498.
19 (a) P. Deng, Y. Yan, S.-D. Wang, Q. Zhang, *Chem. Commun.* 2012, **48**, 2591; (b) D. Asthana, M. R. Ajayakumar, R. P. Pant, P. Mukhopadhyay, *Chem. Commun.* 2012**, 48**, 6475; (c) A. R. Mohebbi, C. Munoz, F. Wudl, *Org. Lett.* 2011**, 13**, 2560; (d) M. Mamada, C. S. Pérez-Bolívar, P. Anzenbacher, *Org. Lett.* 2011, **13**, 4882; (e) D. Hanifi, D. Cao, L. M. Klivansky, Y. Liu, *Chem. Commun.* 2011, **47**, 3454; (f) R. P. Ortiz, H. Herrera, R. Blanco, H. Huang, A. Facchetti, T. J. Marks, Y. Zheng, J. L. Segura, *J. Am. Chem. Soc.* 2010, **132**, 8440; (g) M. Jaggi, C. Blum, B. S. Marti, S. X. Liu, S. Leutwyler, S. Decurtins, *Org. Lett.* 2010, **12**, 1344; (h) M. Jaggi, C. Blum, N. Dupont, J. Grilj, S. X. Liu, J. Hauser, A. Hauser, S. Decurtins, *Org. Lett.* 2009, **11**, 3096; (i) X. C. Li, Y. Xiao, X. H. Qian, *Org. Lett.* 2008, **10**, 2885; (j) A. Wicklein, P. Kohn, L. Ghazaryan, T. Thurn-Albrecht, M. Thelakkat, *Chem. Commun.* 2010, **46**, 2328-2330; (k) Y. Zhang, D. Hanifi, S. Alvarez, F. Antonio, A. Pun, L. M. Klivansky, A. Hexemer, B. Ma, Y. Liu, *Org. Lett.* 2011, **13**, 6528.
20 U. Scherf, *J. Mater. Chem.* 1999, **9**, 1853.
21 H. M. Gajiwala, R. Zand, *Polymer* 2000, **41**, 2009.
22 (a) J. Zhao, G. Li, C. Wang, W. Chen, J. Loo, Q. Zhang, *RSC Adv.* 2013, **3**, 9653; (b) C. Chi, C. Im, G. Wegner, *J. Chem. Phys.* 2006, **124**, 024907.
23 L. Flamigni, E. Baranoff, J. P. Collin, J. P. Sauvage, *Chem. Eur. J.* 2006, **12**, 6592.
24 W. Hong, H. H. Yuan, H. X. Li, X. D. Yang, X. K. Gao, D. B. Zhu, *Org. Lett.* 2011, **13**, 1410.
25 M. L. Tang, T. Okamoto, Z. N. Bao, *J. Am. Chem. Soc.* 2006, **128**, 16002.
26 (a) G. R. Hutchison, M. A. Ratner, T. J. Marks, *J. Am. Chem. Soc.* 2005, **127**, 16866; (b) G. R. Hutchison, M. A. Ratner, T. J. Marks, *J. Am. Chem. Soc.* 2005, **127**, 2339.
27 (a) C. T. Lee, W. T. Yang, R. G. Parr, *Phys.Rev. B* 1988, **37**, 785; (b) H. Qian, W. Yue, Y. Zhen, S. Di Motta, E. Di Donato, F. Negri, J. Qu, W. Xu, D. Zhu, Z. Wang, *J. Org. Chem.*, 2009, **74**, 6275.
28 (a) Z. Q. Lin, P. J. Sun, Y. Y. Tay, J. Liang, Y. Liu, N. E. Shi, L. H. Xie, M. D. Yi, Y. Qian, Q. L. Fan, H. Zhang, H. H. Hng, J. Ma, Q. Zhang, W. Huang, *Acs Nano* 2012, **6**, 5309; (b) B. Yang, J. Xiao, J. I. Wong, J. Guo, Y. Wu, L. Ong, L. L. Lao, F. Boey, H. Zhang, H. Y. Yang, Q. Zhang, *J. Phys. Chem. C* 2011, **115**, 7924; (c) L. A. Estrada, D. C. Neckers, *Org. Lett.* 2011, **13**, 3304; (d) J. Xiao, H. Yang, Z. Yin, J. Guo, F. Boey, H. Zhang, Q. Zhang, *J. Mater. Chem.* 2011, **21**, 1423; (e) J. Xiao, Z. Yin, Y. Wu, J. Guo, Y. Cheng, H. Li, Y. Huang, Q. Zhang, J. Ma, F. Boey, H. Zhang, Q. Zhang, *Small* 2011, **7**, 1242; (f) J. Xiao, Z. Yin, H. Li, Q. Zhang, F. Boey, H. Zhang, Q. Zhang, *J. Am. Chem. Soc.* 2010, **132**, 6926; (g) J. Xiao, Z. Yin, B. Yang, Y. Liu, L. Ji, J. Guo, L. Huang, X. Liu, Q. Yan, H. Zhang, Q. Zhang, *Nanoscale*, 2011, **3**, 4720; (h) J. Xiao, D. Y. Kusuma, Y. Wu, F. Boey, H. Zhang, P. S. Lee, Q. Zhang, *Chem Asian J.* 2011, **6**, 801; (i) Y. Liu, F. Boey, L. L. Lao, H. Zhang, X. Liu, Q. Zhang, *Chem Asian J.* 2011, **6**, 1004; (j) J. Xiao, B. Yang, J. I. Wong, Y. Liu, F. Wei, K. J. Tan, X. Teng, Y. Wu, L. Huang, C. Kloc, F. Boey, J. Ma, H. Zhang, H. Yang, Q. Zhang, *Org. Lett.* 2011, **13**, 3004.
29 (a) J. Zhao, J. I. Wong, C. Wang, J. Gao, V. Z. Y. Ng, H. Y. Yang, S. C. J. Loo, Q. Zhang, *Chem. Asian J.* 2013, **8**, 665; (b) F. Gao, E. Yao, W. Wang, H. Chen, Y. Ma, *Phys. Chem. Chem. Phys.* **2012, 14**, 15321.
30 (a) J. I. Wong, H. Y. Yang, H. Li, T. Chen, H. J. Fan, *Nanoscale* 2012, **4**, 1467; (b) H. Y. Yang, S. F. Yu, C. W. Cheng, S. H. Tsang, H. K. Liang, H. J. Fan, *Appl. Phys. Lett.* 2009, **95**, 201104; (c) H. Y. Yang, S. F. Yu, Y. Y. Hui, S. P. Lau, *Appl. Phys. Lett.* 2010, **97**, 191105; (d) H. Y. Yang, S. F. Yu, H. K. Liang, T. P. Chen, J. Gao, T. Wu, *Opt. Express* 2010, **18**, 15585; (e) H. Y. Yang, S. F. Yu, H. K. Liang, R. G. Mote, C. W. Cheng, H. J. Sun, T. Fan, H. H. Hng, *J. Appl. Phys.* 2009, **106**, 123105.
31 (a) M. Luo, Q. Wang, Z. Y. Wang, *Org. Lett.* 2011, **13**, 4092; (b) Z. Y. Yuan, Y. Xiao, Z. Li, X. H. Qian, *Org. Lett.* 2009, **11**, 2808.